Biomaterials Science

ROYAL SOCIETY OF CHEMISTRY

PAPER

View Article Online
View Journal

Cite this: DOI: 10.1039/d5bm01730k

A click-crosslinked dopamine-functionalized hydrogel for therapeutic delivery of stem cell-derived extracellular vesicles

Joshua S. Copus,[a,b] Ji Hoon Park,[a] Anthony Atala[a,b] and Sang Jin Lee *[a,b]

Stem cell-derived extracellular vesicles (EVs) hold significant promise for tissue regeneration due to their potent therapeutic cargo. However, their clinical translation is hindered by rapid clearance from target sites following systemic or local administration, leading to inefficient delivery and limited therapeutic efficacy. To overcome this critical challenge, we developed a click-crosslinked dopamine-functionalized hyaluronic acid hydrogel system (Dopa-HA) for the sustained and localized delivery of EVs. Dopamine was chemically conjugated to the click-crosslinked hydrogel to enhance the robust immobilization of EVs. The physicochemical properties of this hydrogel system were subsequently characterized, including dopamine functionalization degree, rheological behavior, degradation rates, and *in vitro* protein release profiles. Our investigations revealed that Dopa-HAs (4% and 14%) enable controlled release of model proteins (albumin and cholesterol), with release kinetics directly tunable through adjustments in the degree of dopamine functionalization. Particularly, when loaded with osteogenic stem cell-derived EVs, the Dopa-HA significantly accelerated the osteogenic differentiation of encapsulated stem cells *in vitro*. *In vivo* study in a rat calvarial defect model demonstrated that Dopa-HA markedly enhanced bone regeneration, with Dopa-HA-EV constructs achieving nearly twofold faster defect filling than HA-EV controls. Biodistribution analysis of fluorescently labeled EVs further revealed prolonged local retention at the defect site for up to 10 days post-implantation. This dopamine-functionalized hydrogel platform represents a significant advancement, effectively addressing the challenge of EV delivery by extending their local availability and thereby augmenting therapeutic outcomes.

Received 26th November 2025,
Accepted 10th April 2026

DOI: 10.1039/d5bm01730k

rsc.li/biomaterials-science

1. Introduction

Traditional tissue engineering approaches integrate living cells, biomaterial scaffolds, and bioactive molecules to create functional tissue constructs for repairing or replacing damaged tissues. Despite promising preclinical outcomes, the clinical translation of these cell-based strategies faces considerable challenges.[1,2] A primary impediment is the requirement for high cell densities to produce viable and functional constructs, necessitating extensive, time-consuming, and costly *in vitro* cell expansion. Consequently, cell-free tissue engineering strategies, also known as *in situ* tissue regeneration, have garnered increasing interest.[3–5] These approaches utilize advanced scaffold designs that incorporate bioactive molecules, such as growth factors, peptides, or extracellular vesicles (EVs), to recruit endogenous host cells and stimulate intrinsic tissue regeneration mechanisms.[6–8]

Stem cell-derived EVs have emerged as highly promising therapeutic agents for a wide array of diseases and pathological conditions.[6,9–12] These naturally occurring nanovesicles effectively deliver a diverse payload of bioactive molecules to target cells.[13] Exosomes, a major subpopulation of EVs, are nanoscale lipid bilayer-encapsulated vesicles (30–150 nm in diameter) that play a critical role in paracrine signaling. This signaling is primarily mediated by the transfer of functional proteins, lipids, and nucleic acids, including microRNAs (miRNAs), to recipient cells.[14] Upon internalization, EVs release their molecular cargo, subsequently influencing diverse cellular processes such as proliferation, differentiation, migration, and survival.[15] EVs are readily isolable from the conditioned media of cultured cells.[14] Beyond their cargo versatility, EVs offer several inherent advantages for therapeutic applications, including low immunogenicity, high biological stability, and an intrinsic targeting capacity that promotes preferential uptake by injured or diseased tissues.[16,17] Crucially, the molecular composition and therapeutic efficacy of EVs are

[a]*Wake Forest Institute for Regenerative Medicine, Wake Forest University School of Medicine, Medical Center Boulevard, Winston-Salem, NC 27157, USA.*
E-mail: sang.lee@wfusm.edu
[b]*School of Biomedical Engineering and Sciences, Wake Forest University-Virginia Tech, Winston-Salem, North Carolina, USA*

profoundly influenced by their parent cell source and the environmental conditions of production.[6]

The clinical translation of EV-based therapies is significantly impeded by their poor delivery efficiency. Despite requiring prolonged presence at target sites for optimal therapeutic effects, EVs are rapidly cleared following administration. For instance, a study demonstrated that within a few minutes of systemic injection, the majority of administered EVs preferentially accumulated in clearance organs such as the liver and spleen.[18] While local delivery strategies have shown a modest improvement, reducing hepatic accumulation from approximately 60% to 40%, overall EV bioavailability at the intended target site remains suboptimal.[18] This inherent inefficiency reduces therapeutic efficacy. Therefore, the low retention and inefficient biodistribution of EVs represent a substantial barrier to their clinical translation.

The feasibility of enhancing EV delivery efficiency through the conjugation of target-specific ligands has been established.[19] While this strategy improves targeting, it typically requires the genetic modification of donor cells to induce the expression of specific ligands on the EV surface. As an alternative, direct chemical modification of EV surfaces allows for the post-isolation conjugation of targeting ligands, therapeutic cargo, and polymers. This enhances delivery specificity and circulation stability.[20–22] However, these reactions pose risks such as non-specific protein interactions, inactivation of endogenous surface proteins, membrane destabilization, and cytotoxicity from metal catalysts. These factors collectively compromise EV bioactivity.[23] An ideal solution would involve the integration of EVs within hydrogel systems, thereby enabling localized, sustained release while preserving EV functionality. Such systems could facilitate targeted cellular interactions that promote cell recruitment, migration, and subsequent tissue remodeling, effectively addressing the limitations of current EV delivery strategies.

Sustained delivery of EVs to target tissues has been shown to significantly enhance their therapeutic efficacy throughout the course of treatment.[24] While synthetic hydrogels can facilitate prolonged EV release, they are often limited by poor cell compatibility. Conversely, naturally derived hydrogels offer more favorable cellular microenvironments and can often be formulated into injectable hydrogels. To retain EVs and prevent their premature release, these materials typically require chemical conjugation with affinity ligands or receptors.[25] However, this strategy suffers from several drawbacks: it selectively captures only a subset of EVs bearing appropriate surface markers, and the release of bound EVs is often difficult to regulate due to the irreversible nature of the chemical linkages. Therefore, there is a pressing need for a naturally derived hydrogel system capable of retaining EVs without chemically functionalizing EV surface, thereby avoiding potential damage to the vesicles and preserving their inherent bioactivities.

In this study, we aimed to develop a click-crosslinked hydrogel system designed for the sustained release of EVs through the functionalization of dopamine into its polymeric hydrogel backbone. Dopamine, a key component of mussel adhesive proteins, contains catechol groups known for their strong adhesion properties in aqueous environments, facilitating robust binding to both biological tissues and inorganic surfaces.[26–28] We hypothesized that this dopamine-functionalized hydrogel could significantly enhance EV retention and targeted delivery at specific sites. Additionally, we utilized a bio-orthogonal click chemistry, specifically *via* the reaction between *trans*-cyclooctene (TCO) and tetrazine (Tz) groups for controlled crosslinking process.[29,30] This copper-free click reaction enables swift and efficient gelation under physiological conditions, rendering the system highly amenable to minimally invasive injection. The physicochemical properties of the synthesized dopamine-functionalized hydrogel were thoroughly characterized, including its degree of dopamine functionalization, rheological behavior, and degradation rates. Furthermore, the *in vitro* release profiles were systematically investigated using model proteins to simulate EV release dynamics. Finally, the therapeutic potential and EV retention capabilities of the dopamine-functionalized hydrogel system were evaluated in a rat calvarial defect model.

2. Materials and methods

2.1. Dopamine functionalization

The dopamine-functionalized hyaluronic acid (Dopa-HA) was synthesized *via* carbodiimide coupling, following established protocol.[31] Briefly, 200 kDa HA (LifeCore Biomedical, Chaska, MN) was dissolved in an MES buffer (100 mL, 0.05 M, pH 5.0) at a concentration of 1% w/v in a 250 mL round bottom flask, sealed with a rubber stopper, and stirred for 60 min. EDC (0.951 g, 0.00496 mol) and NHS (0.571 g, 0.00496 mol) were then added at a 1 : 2 molar ratio to HA to activate the carboxyl groups. After 1 h, dopamine hydrochloride (dopamine-HCl) was introduced with different molar ratios to synthesize Dopa-HAs. To prevent dopamine oxidation, nitrogen gas was introduced into the flask. The reaction proceeded overnight and was quenched with 100 mL of DI water. The solution was then dialyzed using 3.4 kDa tubing against DI water for 3 days to remove unreacted materials and excess salts. Finally, the Dopa-HA solution was frozen and lyophilized. All chemical reagents were purchased from Millipore Sigma (Burlington, MA) unless otherwise specified.

2.2. Quantification of dopamine functionalization

To confirm successful dopamine functionalization onto the HA backbone, the chemical structure of the synthesized Dopa-HA was characterized using ^{1}H-NMR spectroscopy. Briefly, 2 mg of Dopa-HA was completely dissolved in 1 mL of deuterated water (D_2O) in a standard NMR glass tube, and spectra were acquired.

For the quantitative analysis, UV-Vis spectroscopy was employed. A standard curve was prepared by dissolving dopamine-HCl in deionized water at concentrations ranging from 0 to 1.5 mM, with absorbance measured at 280 nm. To quantify

the dopamine content within the Dopa-HA hydrogels, synthesized with varying initial molar ratios of dopamine, and a control HA without functionalization were prepared as 10 mg mL^{-1} solutions. Absorbance measurements were performed across a spectral range of 0–450 nm using a UV-2600 UV-Vis spectrophotometer (Shimadzu Scientific Instruments, Durham, NC). The dopamine content in Dopa-HA samples was then quantified by comparing their absorbance at 280 nm to the standard curve. All samples were analyzed in triplicate, and data are presented as mean ± standard deviation.

2.3. Conjugation of click chemistry crosslinkers

To establish click-crosslinked Dopa-HA hydrogels, methyl tetrazine-amine HCl (Tz) and *trans*-cyclooctene-amine HCl (TCO) (BroadPharm, San Diego, CA) were conjugated to Dopa-HA backbones, respectively. Mixing the two components-initiated crosslinking *via* an inverse electron-demand Diels–Alder reaction under physiological conditions. Conjugation was performed at 15, 30, and 60 mmol concentrations relative to the carboxyl groups of Dopa-HA. Dopa-HA was dissolved in 0.1 M MES buffer (pH 5.0) at 10 mg mL^{-1}. EDC and NHS (1 : 1 molar ratio) were added to activate carboxyl groups, followed by 1 h of stirring at room temperature. The solution was then split equally, and either Tz or TCO was added to the respective flasks at specified concentrations. Each reaction proceeded overnight under gentle stirring at room temperature. Afterward, the modified Dopa-HA solutions were dialyzed against deionized water using dialysis tubing with a molecular weight cutoff (MWCO) of 3.4 kDa for 3 days with frequent water changes. The purified products were flash-frozen and lyophilized to obtain dry powders. This method was applied to both low (4%) and high (14%) Dopa-HA hydrogels to generate click-crosslinked hydrogels for subsequent experiments.

2.4. Rheological analysis

To assess the viscoelastic properties of Dopa-HA hydrogels prior to crosslinking, rheological measurements were conducted using a Discovery Hybrid Rheometer-2 (TA Instruments, Wilmington, DE). A 40 mm cone-plate geometry with a 1° angle and a gap height of approximately 100 μm was employed. The average viscosity, storage modulus (G'), and loss modulus (G'') were determined for native HA, 4% Dopa-HA, and 14% Dopa-HA formulations.

To evaluate the effect of crosslinker concentration on gelation kinetics, time sweep experiments were performed immediately after mixing the hydrogel precursors. Measurements were conducted at 37 °C to assess crosslinking behavior. During time sweeps, a constant oscillatory strain of 1% and a frequency of 1 Hz were applied over a duration of 1800 seconds, with data collected at 30-second intervals. Hydrogels were considered fully crosslinked when the loss tangent ($\tan\delta = G''/G'$) dropped below 1, indicating a transition from viscous to elastic-dominant behavior. Following gelation, Modulus (gel stiffness) was evaluated using strain sweep tests conducted within the linear viscoelastic region to ensure characterization of the hydrogel's mechanical response. All measurements were conducted in triplicate (n = 3) for each experimental condition.

2.5. Degradation testing of click-crosslinked Dopa-HA hydrogels

To assess hydrogel stability and its dependence on crosslinking concentration, we characterized the degradation rates. Specifically, the sol fraction, representing the portion of the hydrogel not integrated into the crosslinked network, was quantified. The sol fraction was calculated using eqn (1):

$$S_f = \frac{(W_i - W_d)}{W_i} \quad (1)$$

where W_i is the initial weight and W_d is the dry weight at various time points. A decrease in the sol fraction signifies polymer loss, which directly correlates with the hydrogel's degradation rate. Conversely, the gel fraction, representing the crosslinked portion of the hydrogel, was calculated using eqn (2):

$$G_f = 1 - S_f \quad (2)$$

and it quantified the amount of material remaining within the crosslinked networks that remained intact and did not undergo degradation.

To quantify sol and gel fractions, Dopa-HA-Tz and Dopa-HA-TCO solutions (30 mg mL^{-1} in PBS) were prepared separately, mixed, and incubated at 37 °C for 30 min to allow complete crosslinking. Formed hydrogels were then immersed in fresh PBS and incubated for predetermined degradation periods (1, 3, and 7 days). At each time point, samples were collected, flash-frozen, and lyophilized. The dry mass was measured and compared to the initial hydrated mass to calculate the sol fraction (eqn (1)); the gel fraction was derived accordingly (eqn (2)). All measurements were performed in triplicate (n = 3) for each condition.

2.6. *In vitro* release kinetics assays

To evaluate *in vitro* release kinetics from Dopa-HA hydrogels, low and high concentrations of human serum albumin (2.5 and 12 mg mL^{-1}) and cholesterol (250 and 500 mg mL^{-1}) were incorporated into 4% and 14% Dopa-HA hydrogels, as well as a non-dopamine click-crosslinked HA control. Each 1 mL hydrogel sample was placed in a 6-well plate, submerged in 5 mL deionized water, and incubated at 37 °C on an orbital shaker. Supernatants (1 mL) were collected over 14 days with full media replacement.

Albumin release was quantified using the Pierce™ BCA Protein Assay Kit (Thermo Fisher Scientific, Inc., Waltham, MA). Briefly, 25 μL of each sample or BSA standard was combined with 200 μL of BCA reagent in a 96-well plate, incubated at 37 °C for 30 min, cooled to room temperature, and absorbance was measured at 562 nm. Cholesterol release was assessed using a colorimetric Total Cholesterol Assay Kits (Cell Biolabs, Inc., San Diego, CA). Each 50 μL sample or standard was mixed with 50 μL of reaction reagent, incubated at 37 °C

for 45 min, and absorbance was recorded at 560 nm. Concentrations were determined from standard curves, and data are presented as mean ± SD (n = 6 per group and time point).

2.7. Cell culture

Human placental stem cells (hPSCs; passages 3–5) were isolated from healthy donors with informed consent, under protocols approved by the Institutional Review Board of Wake Forest University School of Medicine (IRB #00056941, Winston-Salem, NC).[32,33] Human PSCs were cultured in growth medium (GM) composed of Dulbecco's Modified Eagle Medium/Nutrient Mixture F-12 (DMEM/F12), supplemented with 10% (v/v) fetal bovine serum (FBS; ScienCell Research Laboratories, Carlsbad, CA), 100 U mL^{-1} penicillin G, and 100 μg mL^{-1} streptomycin (Penicillin–Streptomycin, 10 000 U mL^{-1}). Cells were maintained at 37 °C in a humidified incubator with 5% CO_2. Unless otherwise specified, all cell culture reagents were obtained from Thermo Fisher Scientific, Inc.

2.8. *In vitro* cell viability and proliferation

Cell viability was assessed using Live/Dead staining on hPSC-laden Dopa-HA constructs cultured for 1, 3, and 7 days. Human PSCs were encapsulated at a density of 1.0×10^6 cells per mL by suspending the cell in the hydrogel precursor solution prior to gelation. Following gelation, the hPSC-laden hydrogel constructs were transferred to the GM and maintained at 37 °C in a humidified incubator with 5% CO_2 for up to 7 days. For Live/Dead staining, constructs were rinsed 2–3 times with PBS at room temperature, then incubated with a Live/Dead staining solution containing Calcein AM and propidium iodide (2 : 1 ratio in PBS; 1 mL per well in a 24-well plate) at 37 °C for 15 min. Fluorescence imaging was performed using a Leica TCS LSI Macro Confocal Microscope (Leica Microsystems, Wetzlar, Germany) with excitation wavelengths of 490 nm for live cells and 545 nm for dead cells. Images were processed to visualize viable cells in green and non-viable cells in red. Cell proliferation was evaluated using the AlamarBlue assay. Constructs were incubated in culture medium containing 10% (v/v) AlamarBlue reagent at 37 °C for 3 h. Following incubation, the supernatant was transferred to a 96-well plate, and absorbance was measured at 570 nm with a reference wavelength of 600 nm using a microplate reader.

2.9. Isolation of osteogenic EVs

Osteogenic extracellular vesicles (osteo-EVs) were isolated from hPSCs (passage 11) using a previously established protocol.[6] hPSCs were cultured in T175 flasks and induced to differentiate into the osteogenic lineage over a 21-day period in osteogenic medium (OM) containing 10 nM dexamethasone, 100 μM ascorbic acid, and 2 mM β-glycerophosphate. Following differentiation, the medium was replaced with serum-free culture medium for 72 h to facilitate EV accumulation. Conditioned media were subsequently collected, and EVs were isolated through sequential differential centrifugation and filtration. The resulting osteo-EVs were comprehensively characterized as described in our previous study.[6]

2.10. *In vitro* osteogenic differentiation of hPSCs in Dopa-HA constructs

To evaluate the efficacy of the Dopa-HA hydrogel system, two hydrogel formulations were prepared for comparison: a 14% (w/v) Dopa-HA hydrogel and a click-crosslinked HA hydrogel without dopamine functionalization. Each formulation was loaded with 150 μg mL^{-1} of osteo-EVs. Human PSCs were encapsulated at a density of 1.0×10^6 cells per mL by suspending them in the hydrogel solution prior to gelation. The cell-laden HA hydrogels were maintained in OM for 21 days. Alkaline phosphatase (ALP) activity assays were conducted on days 7 and 14 to assess early osteogenic commitment. Mineral deposition was evaluated *via* Alizarin Red S staining on days 7, 14, and 21. The click-crosslinked HA constructs without dopamine functionalization and osteo-EVs cultured in GM served as a negative control.

For ALP assay, samples were washed with PBS, then homogenized and lysed using Triton X-100 in accordance with the manufacturer's protocol (One-Step Kit; Thermo Fisher Scientific, Inc.). ALP activity was assessed using *p*-nitrophenyl phosphate (*p*NPP) as the substrate. The enzymatic conversion of *p*NPP to p-nitrophenol, indicative of ALP activity, was quantified spectrophotometrically. Measurements were performed on days 7 and 14, with n = 4 for each time point and experimental group.

For histological analysis, samples were rinsed with PBS and fixed in 10% neutral-buffered formalin overnight at 4 °C. Following fixation, specimens were dehydrated in 70% ethanol, paraffin-embedded, sectioned at a thickness of 7 μm, and mounted on glass slides. For Alizarin Red S staining, tissue sections were deparaffinized, rehydrated to 50% ethanol, rinsed with distilled water, and stained with 2% Alizarin Red S (pH 4.2) for 1 min. Slides were counterstained with light green, treated sequentially with acetone and acetone–xylene (1 : 1), and cleared in xylene. Coverslips were applied, and imaging was performed using a Leica DM4000B microscope.

2.11. *In vivo* animal study

Male Lewis rats (300–500 g) were used in accordance with protocols approved by the Institutional Animal Care and Use Committee (IACUC) at Wake Forest University. The experimental design included two treatment groups: one receiving 14% Dopa-HA hydrogel loaded with 150 μg mL^{-1} of osteo-EVs, and the other receiving click-crosslinked HA hydrogel (non-Dopa-functionalized) loaded with the same EV concentration. To evaluate EV biodistribution, all osteo-EVs were fluorescently labeled with DiIC18(7) 1,1′-dioctadecyl-3,3,3′,3′-tetramethylindotricarbocyanine Iodide (DiR′) following the manufacturer's protocol (Sigma-Aldrich, St Louis, MO).

For implantation, anesthesia was induced and maintained with 3% isoflurane delivered *via* a custom-designed nosecone. Animals were placed on heated pads and stabilized in a stereo-

taxic frame throughout the procedure. A midline scalp incision was made to expose the calvarium, followed by careful removal of the periosteum. A cranial defect (4 mm diameter) was created on the parietal bone using a dental burr. The HA-EV or Dopa-HA-EV hydrogels were applied to the defect site. Following implantation, incisions were closed using absorbable sutures and skin adhesive. Preoperative analgesics included bupivacaine (8 mg kg^{-1}), buprenorphine (0.05 mg kg^{-1}), meloxicam (2 mg kg^{-1}), and famotidine (0.5 mg kg^{-1}). Postoperative monitoring involved close observation for recovery and assessment of neurological status. Animals without treatment served as controls.

2.12. Biodistribution analysis

The biodistribution of DiR-labeled osteo-EVs was evaluated using the IVIS® Lumina XR imaging system (PerkinElmer, Waltham, MA). Fluorescent imaging was conducted under near-infrared (NIR) excitation/emission settings with an indocyanine green (ICG) filter. Animals (n = 3 per time point) were anesthetized using 1–5% isoflurane during imaging sessions. Fluorescent signals were captured on days 1, 3, 7, and 10 following implantations.

2.13. Computed tomography (CT) analysis

New bone formation was evaluated using computed tomography (CT) imaging. Animals were euthanized at predetermined time points (2, 4, and 8 weeks post-implantation) *via* CO_2 asphyxiation followed by bilateral thoracotomy, in accordance with the IACUC protocol. CT imaging was performed using the Vimago™ High-Definition CT Imaging System (Epica Medical Innovations, San Diego, CA) at a voxel resolution of 90 μm. For each experimental group and time point, five animals were assessed (n = 5). Image reconstruction, volumetric quantification, and 3D rendering were conducted using 3D Slicer (https://www.slicer.org), an open-source platform for medical image analysis and visualization.

2.14. Histological examination

Retrieved samples were fixed in 10% neutral buffered formalin for 48 h. Following fixation, specimens were decalcified using Richard Allan Scientific Decalcifying Solution per the manufacturer's protocol (TermoFisher Scientific, Inc.). Decalcified tissues were then sectioned into 12 μm-thick slices and stained with modified Tetrachrome staining to detect new bone formation. Histological imaging was carried out using a Leica DM4000B microscope.

2.15. Statistical analysis

Continuous variables are expressed as mean ± standard deviation (SD). Prior to statistical analysis, data were assessed for normality using the Shapiro–Wilk test and for homogeneity of variance using Levene's test. Differences among groups were evaluated using a one-way analysis of variance (ANOVA). When the omnibus F-test indicated statistical significance ($p < 0.05$), Tukey's HSD (Honestly Significant Difference) *post-hoc* test was applied to identify specific pairwise differences while controlling for the Type I error rate. All statistical analyses were performed using GraphPad Prism 10.0.

3. Results

3.1. Click-crosslinked dopamine-functionalized HA hydrogels

To develop the click-crosslinked hydrogel platform for controlled release of bioactive molecules, dopamine was covalently conjugated to the HA backbone, followed by the covalently binding of tetrazine (Tz) and *trans*-cyclooctene (TCO), respectively, for click chemistry to form hydrogels. Fig. 1A shows the schematic diagram of the resulting Dopa-HA hydrogel and its proposed mechanism for controlled release of bioactive molecules, including EVs. Successful conjugation was confirmed *via* ^{1}H NMR spectroscopy (Fig. 1B). Native HA displayed characteristic peaks at 1.95–2.0 ppm, corresponding to the *N*-acetyl group, and at 2.8–3.7 ppm for *N*-acetyl-D-glucosamine. The introduction of dopamine, Tz, and TCO resulted in distinct new peaks: 6.7–7.2 ppm for dopamine's catechol protons, 7.0–7.2 ppm and 8.0–8.2 ppm for Tz, and 5.5–6.0 ppm for TCO, respectively. These observations confirmed the stepwise and successful functionalization of HA with dopamine and the bio-orthogonal reactive groups.

To quantitatively assess dopamine functionalization efficiency, UV-Vis spectroscopy was performed using a dopamine standard curve ranging from 0 to 1.5 mM (Fig. 1C). The degree of dopamine substitution was tunable based on the dopamine concentration, yielding two distinct groups: low and high Dopa-HA, with functionalization degrees of 4.14 ± 2.22% and 14.07 ± 1.66%, respectively (Fig. 1D). These spectral changes collectively demonstrate the sequential and successful modification of HA with dopamine and the reactive click pair.

3.2. Characterization of in click-crosslinked Dopa-HA hydrogels

The gelation behavior of click-crosslinked Dopa-HA hydrogels was assessed before and after the click reaction. Macroscopic observations confirmed the transition from the pre-gel solution to a solidified hydrogel (Fig. 2A). Rheological assessments were conducted to determine the influence of varying dopamine functionalization levels (0%, 4%, and 14%) on the rheological properties of Dopa-HA hydrogels. Average viscosity revealed a substantial increase corresponding to dopamine content, with Dopa-HA (14%) exhibiting a viscosity of 931.9 cPs, compared to 333.8 cPs for Dopa-HA (4%) (Fig. 2B). Further rheological analysis demonstrated that both the storage modulus (Fig. 2C) and loss modulus (Fig. 2D) increased proportionally with higher dopamine functionalization. These findings suggest that dopamine functionalization enhances the viscoelastic behavior of Dopa-HA hydrogels.

To examine the effect of crosslinker concentration on the physical characteristics of Dopa-HA hydrogels, various amounts of TCO and Tz crosslinkers (15, 30, and 60 mmol) were tested. As In Fig. 2E, gelation time was strongly depen-

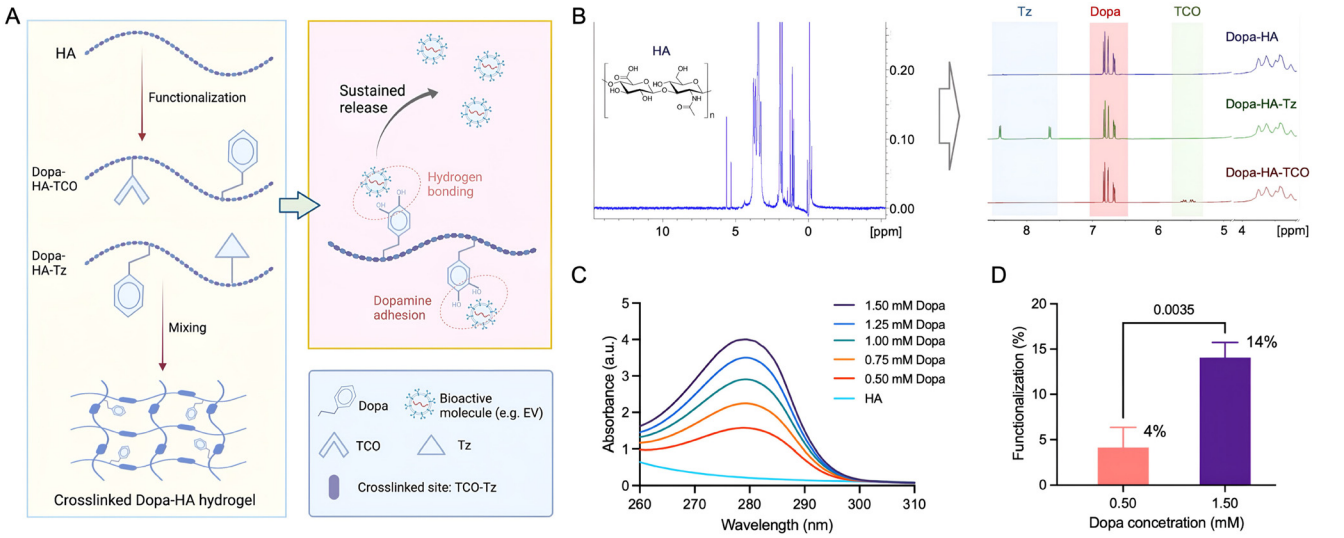

Fig. 1 (A) Schematic representation of a click-crosslinked Dopa-HA hydrogel designed for the delivery of bioactive molecules. (B) ^{1}H-NMR spectra showing the functionalization of Dopa-HA, Dopa-HA-Tz, and Dopa-HA-TCO. (C) UV-Vis spectra presenting peak variations in dopamine absorbance corresponding to different dopamine concentrations used during synthesis. (D) Quantitative analysis of average dopamine functionalization percentages achieved by conjugating selected amounts (0.5 and 1.5 mM) of dopamine (n = 3). All data are represented as mean ± SD.

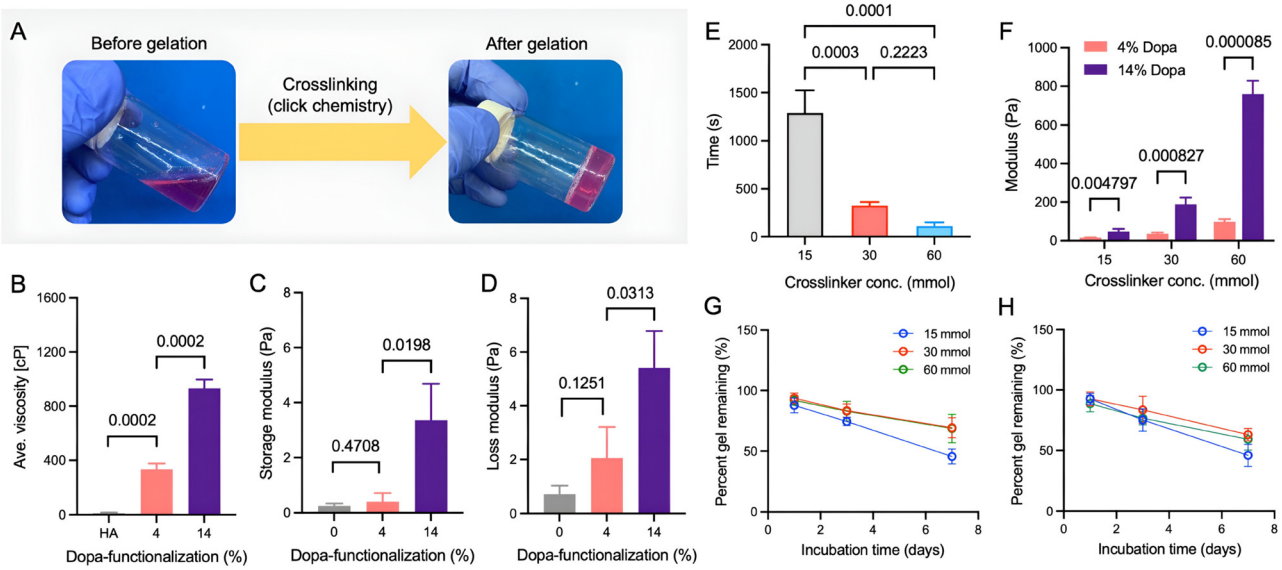

Fig. 2 (A) Gross appearance of the Dopa-HA hydrogel system before and after gelation. (B) Effect of dopamine functionalization on the rheological properties of Dopa-HA hydrogels: (B) average viscosity (n = 3), (C) storage modulus (n = 3), and (D) loss modulus (n = 3). (E) Effect of crosslinking time on Dopa-HA (14%) hydrogels with varying amounts of conjugated crosslinker (n = 3). (F) Modulus (gel stiffness) of crosslinked Dopa-HA hydrogels as a function of crosslinker concentration (n = 3). Degradation profiles of Dopa-HA hydrogels with varying crosslinker concentrations: (G) 4% and (H) 14% Dopa-functionalization (n = 3). All data are represented as mean ± SD.

dent on crosslinker concentration, with higher concentrations significantly accelerating the transition to a fully crosslinked network. Specifically, the formulation containing 15 mmol of crosslinker had an average gelation time of 1291.6 ± 232.7 seconds, while the 30 mmol and 60 mmol formulations gelled in 323.6 ± 37.8 seconds and 111.2 ± 37.7 seconds, respectively. These results confirm the critical role of crosslinker concentration in gelation process. However, dopamine functionalization did not influence the gelation process.

Following gelation analysis, six distinct hydrogel formulations were synthesized by 4% and 14% Dopa-HAs with TZ and TCO (15, 30, and 60 mmol). These formulations were

subsequently evaluated for their mechanical properties and degradation behavior. Modulus (gel stiffness) was characterized through strain sweep tests performed within the linear viscoelastic region (Fig. 2F). For hydrogels functionalized with 14% dopamine, the modulus increased substantially with higher crosslinker concentrations, rising from 47.8 ± 13.3 Pa at 15 mmol to 189.1 ± 34.4 Pa at 30 mmol and reaching 759.7 ± 69.2 Pa at 60 mmol. In contrast, hydrogels with 4% dopamine showed considerably lower modulus, registering moduli of 15.9 ± 1.2 Pa, 36.1 ± 6.8 Pa, and 98.1 ± 13.7 Pa at 15, 30, and 60 mmol, respectively. These observations highlight the significant contribution of dopamine functionalization to hydrogel stiffness, complementing the effects of increasing crosslinker concentration.

Degradation profiles were assessed over a 7-day period. All formulations exhibited progressive degradation, though no direct correlation with crosslinker concentration was observed. 4% Dopa-HA hydrogels retained gel fractions of 45.5 ± 6.1%, 69.3 ± 8.3%, and 68.6 ± 11.8% for the 15, 30, and 60 mmol formulations, respectively (Fig. 2G). 14% Dopa-HA hydrogels demonstrated slightly varied retention, with gel fractions of 45.8 ± 9.1%, 63.0 ± 5.2%, and 59.2 ± 8.9% for the same crosslinker concentrations (Fig. 2H). These results suggest that degradation behavior is likely governed by factors such as hydrolysis of the HA backbone or crosslinker chemistry, rather than dopamine content alone. While dopamine functionalization had a pronounced impact on mechanical properties, its influence on degradation rates appeared minimal.

3.3. *In vitro* release kinetics

The albumin release assay exhibited a characteristic initial burst within the first 3 h post-loading, indicating non-covalently associated albumin species – either freely dispersed or transiently entrapped within the hydrogel network without stable interactions with the matrix surface. Following this early phase, the release profile conformed to first-order kinetics, demonstrating a progressive and sustained release over a 14-day period. Comparative analysis revealed statistically significant differences in release behavior between Dopa-HA hydrogels and the non-functionalized HA control. Specifically, 4% Dopa-HA hydrogels sustained albumin release through day 10, while 14% Dopa-HA hydrogels exhibited an extended release profile lasting up to day 14. This prolonged release was observed consistently across both low and high albumin loading conditions – 2.5 mg mL^{-1} (Fig. 3A) and 12 mg mL^{-1} (Fig. 3B) – indicating that the release kinetics were primarily governed by the degree of dopamine functionalization rather than the initial protein concentration.

The cholesterol release assay similarly demonstrated sustained release profiles under both low (250 μg mL^{-1}, Fig. 3C)

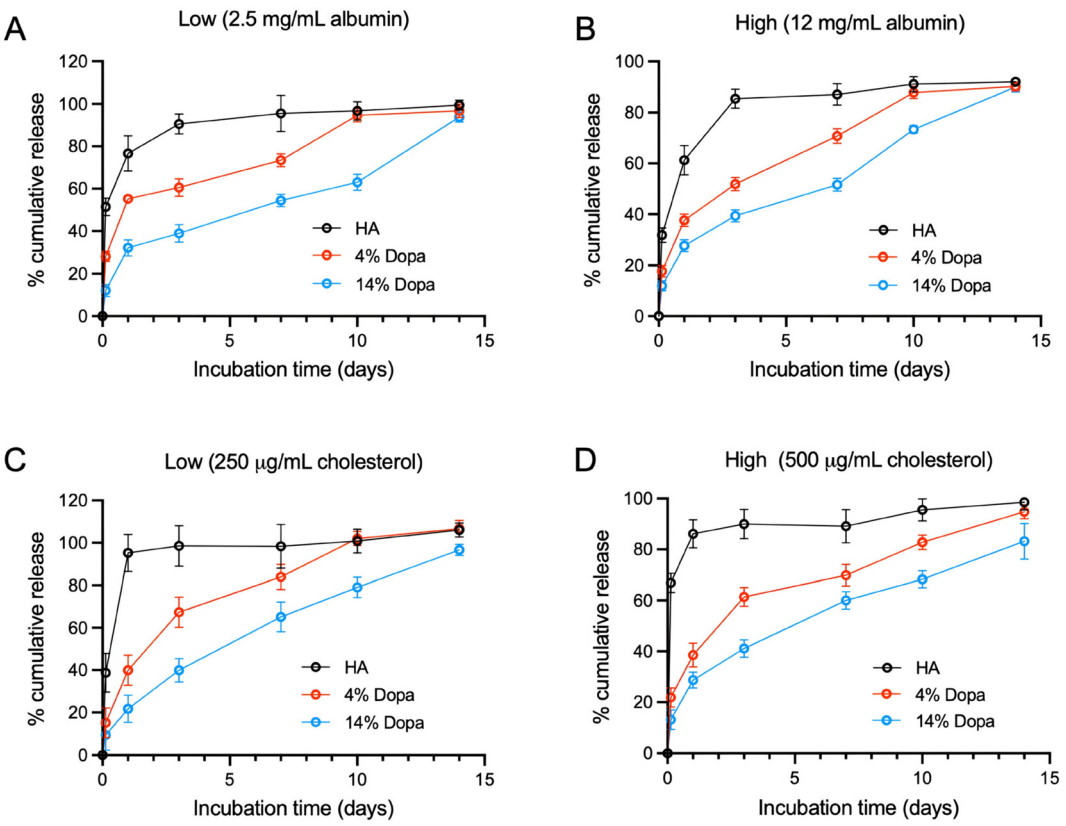

Fig. 3 Release kinetics of model biomolecules from Dopa-HA hydrogels with varying dopamine functionalization: (A) 2.5 mg mL^{-1} albumin (n = 6), (B) 12 mg mL^{-1} albumin (n = 6), (C) 250 μg mL^{-1} cholesterol (n = 6), and (D) 500 μm mL^{-1} cholesterol (n = 6). All data are represented as mean ± SD.

and high (500 μg mL^{-1}, Fig. 3D) loading conditions, with release extending through 14-day period. Consistent with the albumin release data, the Dopa-HA hydrogels with higher dopamine functionalization exhibited enhanced cholesterol retention. Under low cholesterol loading, an initial burst release was observed; however, 4% Dopa-HA hydrogels showed statistically significant release only until day 7, whereas 14% Dopa-HA hydrogels maintained sustained release through day 14. These results highlight the influence of dopamine-mediated interactions on protein retention and release kinetics, suggesting enhanced matrix-protein affinity and prolonged release profiles in Dopa-functionalized systems.

3.4. *In vitro* cell viability and proliferation

To assess cell viability within Dopa-HA hydrogels, Live/Dead staining was conducted on constructs containing 4% and 14% dopamine functionalization, cultured under GM conditions. Imaging performed on days 1, 3, and 7 revealed consistently high cell viability, with minimal presence of dead cells across all time points (Fig. 4A). Quantitative analysis further confirmed that encapsulated hPSCs remained viable and actively proliferated when maintained in GM (Fig. 4B). Additionally, the proliferation of hPSCs encapsulated within 14% Dopa-HA hydrogels revealed continuous expansion throughout the 14-day culture period (Fig. 4C). These findings highlighted the excellent cytocompatibility of Dopa-HA hydrogels and their potential as a supportive matrix for long-term cell encapsulation, maintenance, and growth.

3.5. *In vitro* osteogenic differentiation

Human PSCs encapsulated within click-crosslinked HA hydrogels were subjected to osteogenic differentiation for up to 21 days. The Dopa-HA-EV hydrogels with osteo-EVs demonstrated significantly elevated ALP activity, reaching 21 U L^{-1} and 28 U L^{-1} on days 7 and 14, respectively, compared to 16 U L^{-1} and 23 U L^{-1} in the HA-EV group (Fig. 5A). Furthermore, EVs incorporated into the Dopa-HA-EV hydrogels markedly enhanced calcium deposition, as evidenced by Alizarin Red staining and quantitative analysis (Fig. 5B and C). The Dopa-HA-EV group exhibited substantially larger stained areas (10% and 43% at days 7 and 14) relative to the HA-EV group (6% and 24%) and the control group (0.4% at all time points), indicating a pronounced enhancement of osteogenic differentiation mediated by osteo-EVs within the Dopa-HA-EV hydrogels. These results suggest that dopamine functionalization effectively modulates EV retention within the hydrogel, facilitating prolonged bioactivity while maintaining efficient EV uptake by encapsulated cells.

3.6. *In vivo* rat calvarial bone defect model

In vivo studies demonstrated that dopamine functionalization significantly prolonged the retention of EVs at the target site, as evidenced by DiR-labeled EV biodistribution analysis (Fig. 6A). At day 10, the Dopa-HA-EV hydrogel group exhibited a radiant efficiency of 2×10^8, whereas no detectable signal was observed at the defect site in the HA-EV group, indicating rapid clearance and limited EV retention in the absence of

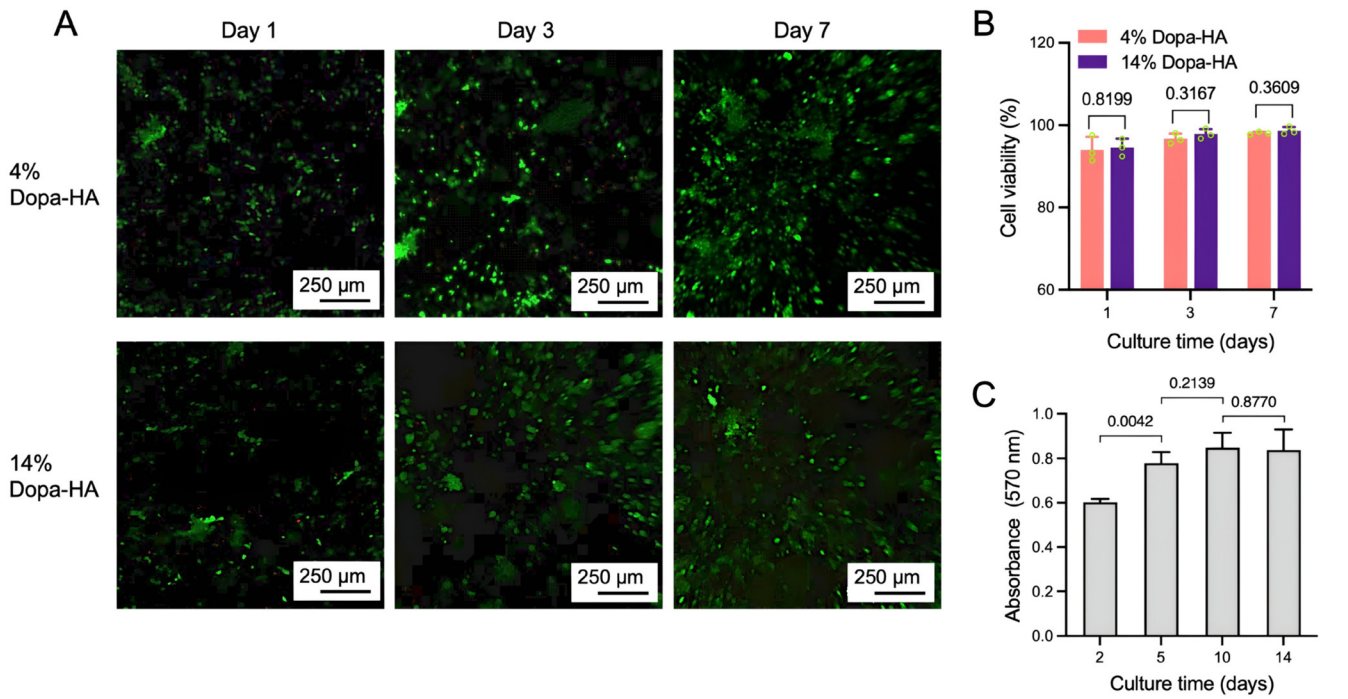

Fig. 4 *In vitro* viability and proliferation of hPSCs encapsulated in Dopa-HA hydrogels with 4% and 14% dopamine functionalization at 1, 3, and 7 days of culture: (A) Live/Dead stained fluorescence images and (B) quantitative analysis of cell viability (%) (n = 3). (C) Cell proliferation of hPSCs encapsulated in Dopa-HA hydrogels with 14% Dopa-functionalization by AlamarBlue assay (n = 3). All data are represented as mean ± SD.

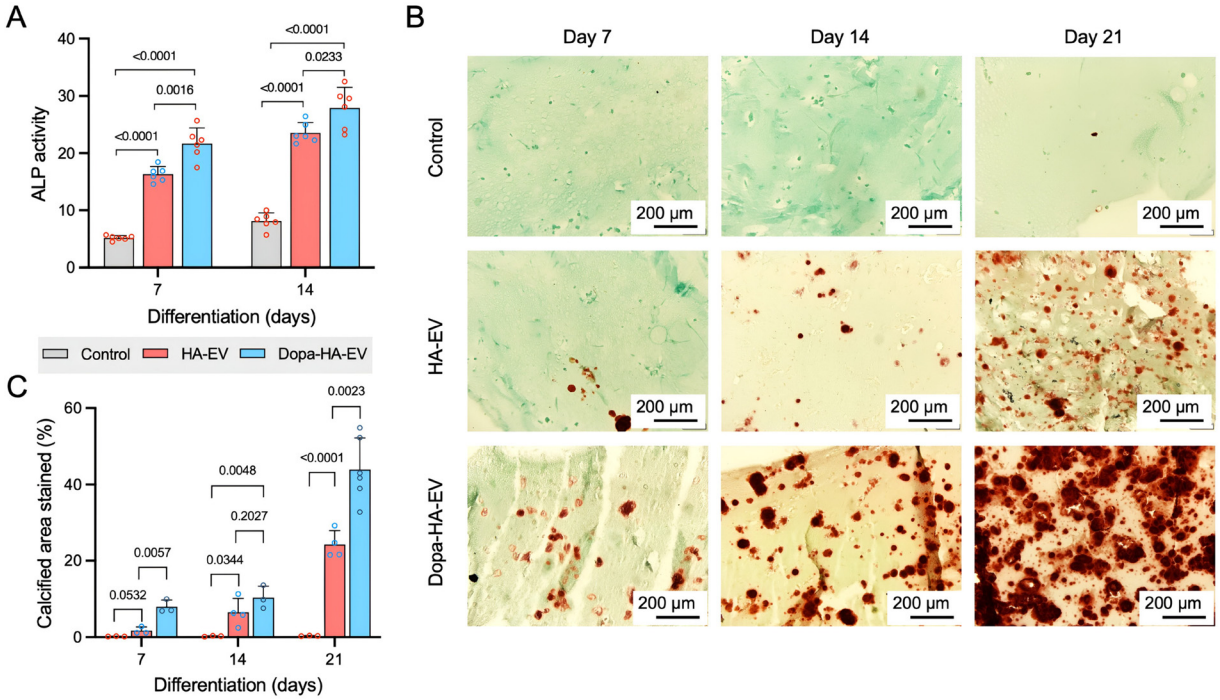

Fig. 5 *In vitro* osteogenic differentiation of hPSCs encapsulated in Dopa-HA hydrogels with 14% dopamine functionalization and 150 μg mL^{-1} of osteo-EVs. (A) ALP activity assessed at 7 and 14 days of differentiation (n = 6). (B) Alizarin Red staining images at 7, 14, and 21 days of differentiation. (C) Quantification of calcified regions within the HA-Dopa hydrogels based on Alizarin Red staining (n = 6). All data are represented as mean ± SD.

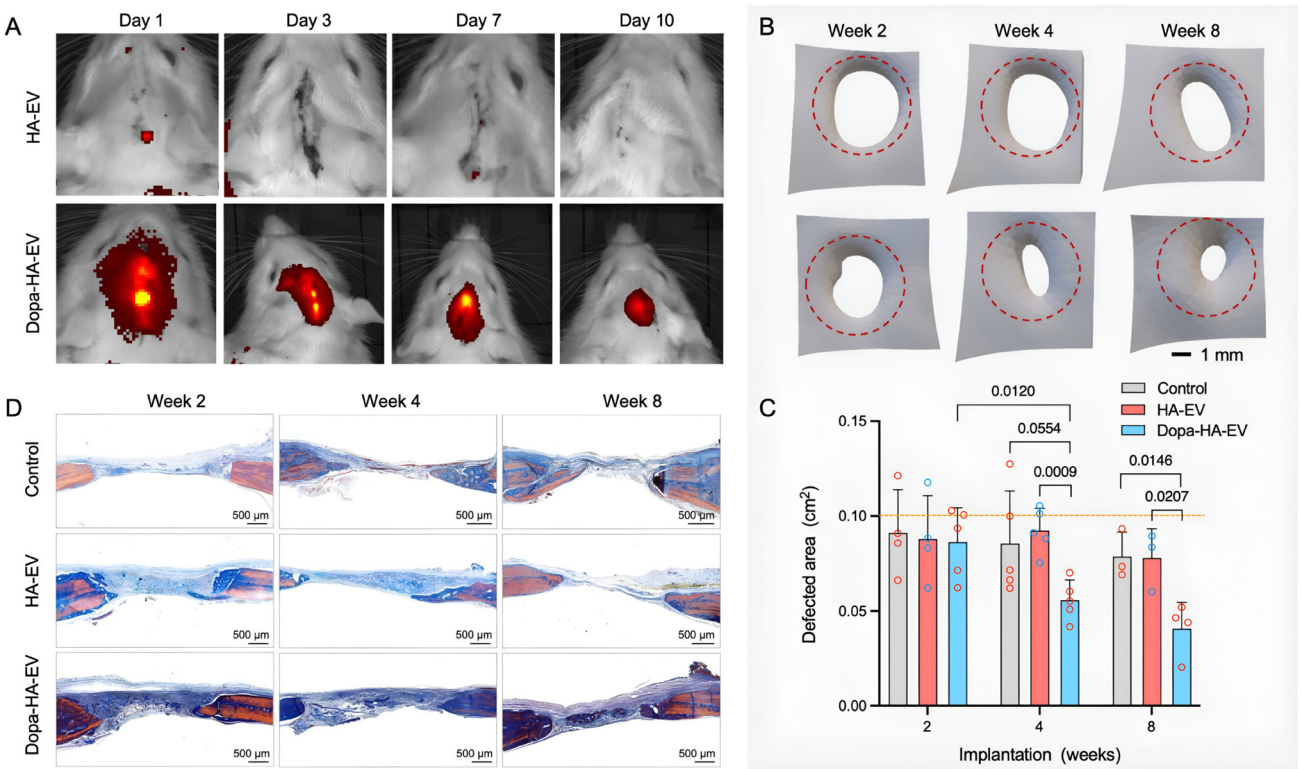

Fig. 6 *In vivo* validation of HA-Dopa hydrogels for calvarial bone reconstruction. (A) Biodistribution of DiR-labeled EVs embedded within Dopa-HA hydrogels. (B) CT reconstruction of defect sites at 2, 4, and 8 weeks post-treatment. (C) Quantitative analysis of defect area at corresponding time points (n = 5). All data are represented as mean ± SD. (D) Histological evaluation using modified Tetrachrome staining, with newly formed bone (mineralized bone matrix, red) and osteoid (unmineralized bone matrix, blue). SI Fig. S1 provides high magnification images.

dopamine functionalization. This sustained localization of EVs in the Dopa-HA-EV group correlated with improved therapeutic outcomes, as reflected by a significant reduction in defect size compared to the HA-EV group (Fig. 6B and C). The initial defect area of 0.12 cm^2 decreased to 0.086 cm^2 in the Dopa-HA-EV group and 0.088 cm^2 in the HA-EV group after two weeks. In non-treatment controls, residual defect sizes averaged 0.085 cm^2 and 0.091 cm^2 for the Dopa-HA-EV and HA-EV groups, respectively, suggesting that the presence of osteo-EVs within the Dopa-HA-EV contributed to enhanced bone regeneration. Histological analysis further confirmed increased new bone formation in defects treated with Dopa-HA hydrogels (Fig. 6D). Tetrachrome staining confirmed the presence of mineralized bone (red) and unmineralized osteoid (blue) within the defect area. The Dopa-HA-EV group exhibited more extensive bone formation compared with the HA-EV and control groups (SI Fig. S1).

4. Discussion

The delivery of bioactive molecules such as proteins, nucleic acids, and EVs *via* hydrogel-based systems holds significant promise for therapeutic applications, particularly in the field of tissue engineering. However, achieving controlled and sustained release remains a major challenge, largely due to the limited intrinsic interactions between these molecules and the hydrogel matrix. EVs, in particular, lack specific surface motifs that facilitate stable binding or retention within conventional hydrogel systems, resulting in rapid diffusion and diminished therapeutic efficacy.[18] To address this limitation, the present study employed dopamine functionalization of HA-based hydrogels to enhance molecular retention. The incorporation of catechol groups introduced by dopamine enables non-covalent interactions such as hydrogen bonding and π–π stacking with bioactive molecules, thereby improving their immobilization within the hydrogel network.[34] This strategy facilitates sustained release and preserves bioactivity, ultimately enhancing the therapeutic potential of EVs and other biomolecules delivered through the hydrogel platform.

In this study, HA was selected due to its biocompatibility and abundance of carboxyl groups, which offer versatile sites for chemical modification.[35] This structural framework enables the conjugation of dopamine molecules and crosslinkers, allowing for the development of hydrogels with highly tunable physicochemical properties. Dopamine functionalization was achieved through carbodiimide chemistry using EDC/NHS coupling, which facilitates the formation of covalent amide bonds between the primary amine groups of dopamine and the activated carboxyl groups on the HA backbone. To investigate the influence of dopamine content on hydrogel behavior, two variants of dopamine-functionalized HA (4% Dopa-HA and 14% Dopa-HA) were synthesized, representing low and high degrees of functionalization, respectively. These Dopa-HAs were subsequently modified with click chemistry-compatible crosslinkers, enabling the formation of click-crosslinked hydrogels. This approach provides a robust platform for studying how dopamine content affects both the release kinetics of encapsulated bioactive molecules and the mechanical and structural properties of the hydrogel network.

Critically, our approach facilitates controlled retention of bioactive molecules through non-specific adhesive interactions mediated by dopamine, eliminating the need for specific ligand–receptor binding. This enables the effective incorporation of model molecules such as albumin and cholesterol into the hydrogel, regardless of their surface chemistry or binding motifs. Both 4% Dopa-HA and 14% Dopa-HA hydrogels demonstrated statistically significant improvements in retention compared to the HA control group, independent of the initial protein loading concentration. Release profiles revealed an initial burst phase followed by a sustained release that approximates first-order kinetics, with protein release gradually increasing over a two-week period. Importantly, the release kinetics of the Dopa-HA hydrogels can be modulated by varying the degree of dopamine functionalization. This tunability offers a versatile platform for tailoring hydrogel performance to meet the specific demands of diverse biomedical applications, including drug delivery and tissue regeneration.

Previously,[6] we isolated EVs from human bone marrow-derived mesenchymal stem cells (hBMSCs; passages 3–5) and hPSCs (passage 11). In accordance with MISEV guidelines, EVs were characterized *via* transmission electron microscopy (TEM), confirming typical cup-shaped morphology, and nanoparticle tracking analysis (NTA), verifying a size distribution of 50–200 nm. Notably, hPSCs yielded significantly higher protein and lipid concentrations than hBMSCs, suggesting superior scalability for EV production. Next-generation sequencing (NGS) identified 306 miRNAs within the EV cargo; 64 miRNAs associated with osteogenic pathways were significantly enriched in hPSC-derived EVs. While miR-10b was more abundant in hBMSC-EVs, hPSC-EVs expressed high levels of osteopromotive miR-146, miR-515, and miR-520a. Functional assays demonstrated that EVs harvested at the late stage of differentiation (Day 21) exhibited enhanced capacity for mineral deposition compared to early-stage counterparts. Consequently, hPSC-derived EVs represent a functionally equivalent, high-yield alternative to hBMSC-EVs for bone tissue engineering.

The *in vitro* evaluations demonstrated that the Dopa-HA hydrogel system effectively supported both the encapsulation of viable cells and sustained delivery of osteogenic bioactive molecules capable of tissue formation. Live/Dead staining revealed no cytotoxicity toward encapsulated hPSCs, while viability and proliferation assays confirmed that the cells remained metabolically active and continued to proliferate under GM conditions. Osteogenic differentiation assays further validated that constructs containing Dopa-HA hydrogels exhibited significantly enhanced calcium deposition compared to HA controls, indicating superior osteoinductive potential. This enhancement is attributed to the dopamine-mediated retention of osteo-EVs within the hydrogel. This enhancement suggests that dopamine functionalization plays

a critical role in modulating EV release kinetics, preventing premature diffusion while maintaining bioactivity. Importantly, dopamine-mediated retention did not impair the ability of encapsulated cells to internalize EVs, a limitation commonly associated with other conjugation strategies that may hinder vesicle uptake. These findings highlight the multifunctionality of the Dopa-HA hydrogel system, which combines cytocompatibility, tunable release kinetics, and efficient molecular delivery.

The *in vivo* rat calvarial defect model provided robust validation of our hypothesis that dopamine functionalization enhances the localized retention and sustained release of osteo-EVs. Fluorescence imaging of DiR-labeled EVs demonstrated prolonged signal persistence at the defect site in animals treated with Dopa-HA hydrogels, indicating effective EV retention compared to non-functionalized HA controls. CT analysis revealed a statistically significant reduction in defect size in the Dopa-HA group, emphasizing the superior regenerative efficacy of the Dopa-functionalized hydrogel. Additionally, histological evaluation further confirmed enhanced osteogenesis, with markedly increased new bone formation observed in the Dopa-HA-treated defects relative to controls. Collectively, these findings demonstrate that Dopa-HA hydrogels facilitate sustained EV delivery at the site of injury, thereby amplifying their therapeutic potential for bone regeneration. The integration of dopamine chemistry into the hydrogel matrix not only improves EV retention but also preserves their bioactivity, positioning this platform as a promising candidate for translational applications in tissue engineering.

A key advantage of this hydrogel system lies in its ability to retain EVs without requiring chemical modification of the EV surface. This avoids a major limitation of alternative delivery strategies that may compromise vesicle integrity or alter cellular internalization pathways, thereby preserving the native bioactivity and uptake mechanisms of EVs. The Dopa-functionalized hydrogel also offers a minimally invasive platform for sustained EV delivery, with tunable release kinetics. Modulation of the crosslinking density enables precise control over hydrogel degradation rates. Moreover, the non-specific binding mechanism and modular architecture of the hydrogel extend its utility beyond bone tissue engineering, making it suitable for a broad range of therapeutic applications.

Although this study demonstrates effective EV delivery using the Dopa-functionalized hydrogel system, it is constrained by short-term evaluation in a small-animal model. Future investigations will comprehensively map EV distribution within the Dopa-HA hydrogel, quantify EV-cell internalization and associated downstream signaling, and assess the long-term maintenance of EV bioactivity and regenerative efficacy in relevant preclinical animal models.

5. Conclusions

The Dopa-functionalized HA hydrogel system represents a versatile and biologically responsive platform for the sustained delivery of EVs. By leveraging dopamine-mediated retention without chemically altering the EV surface, this approach preserves EV integrity and cellular uptake pathways, overcoming critical limitations of conventional delivery methods. *In vivo* studies conducted in a rat calvarial defect model demonstrated enhanced bone regeneration. Utilizing CT imaging analysis and qualitative histomorphological assessment, significant defect closure and increased new bone formation were observed in the Dopa-HA-treated groups. These outcomes were supported by prolonged EV retention at the defect site and tunable release kinetics, achieved through controlled crosslinking and dopamine functionalization. The Dopa-functionalized hydrogel's non-specific binding mechanism extends its applicability beyond bone tissue engineering, offering promise for broader therapeutic applications. Together, these findings position the Dopa-HA hydrogel for EV-based regenerative therapies, combining precision delivery, biocompatibility, and structural adaptability.

Author contributions

J. S. Copus: conceptualization, investigation, visualization, formal analysis, data curation, methodology, writing – original draft. J. H. Park: conceptualization, investigation, methodology. A. Atala: conceptualization, resources, funding acquisition, writing – review and editing. S. J. Lee: conceptualization, resources, supervision, funding acquisition, validation, investigation, project administration, writing – review and editing.

Conflicts of interest

The authors declare no conflicts of interest.

Data availability

The data that support the findings of this study are available within the article and raw data are available from the corresponding author upon reasonable request.

Supplementary information (SI) is available. Modified Tetrachrome staining to detect newly formed bone (red, mineralized bone matrix) and osteoid (blue, unmineralized bone matrix). See DOI: https://doi.org/10.1039/d5bm01730k.

Acknowledgements

The authors thank Ms Denethia Green for her assistance with histological analysis and Dr Kyung Kwan Lee for performing ^{1}H-NMR analysis. This work was supported by the National Institute of Biomedical Imaging and Bioengineering (Grant No. 1P41EB023833-01) and, in part, by the National Center for Advancing Translational Sciences (Grant No. UM1TR004929), the National Institutes of Health.

References

1 T. Hoffman, A. Khademhosseini and R. Langer, *Tissue Eng., Part A*, 2019, **25**, 679–687.
2 A. Atala, *Tissue Eng., Part A*, 2024, **30**, 5–13.
3 S. J. Lee, A. Atala and J. J. Yoo, *In situ tissue regeneration: host cell recruitment and biomaterial design*, Academic Press, 2016.
4 I. K. Ko, S. J. Lee, A. Atala and J. J. Yoo, *Exp. Mol. Med.*, 2013, **45**, e57.
5 S. J. Lee, M. Van Dyke, A. Atala and J. J. Yoo, *Rejuvenation Res.*, 2008, **11**, 747–756.
6 E. Pishavar, J. S. Copus, A. Atala and S. J. Lee, *Tissue Eng., Part A*, 2021, **27**, 1044–1054.
7 I. K. Ko, Y. M. Ju, T. Chen, A. Atala, J. J. Yoo and S. J. Lee, *FASEB J.*, 2012, **26**, 158–168.
8 N. Kim, J. J. Yoo, A. Atala and S. J. Lee, *FASEB J.*, 2016, **30**, 1198–1206.
9 K.-S. Park, E. Bandeira, G. V. Shelke, C. Lässer and J. Lötvall, *Stem Cell Res. Ther.*, 2019, **10**, 1–15.
10 A. K. Batsali, A. Georgopoulou, I. Mavroudi, A. Matheakakis, C. G. Pontikoglou and H. A. Papadaki, *J. Clin. Med.*, 2020, **9**, 856.
11 L. R. Galieva, V. James, Y. O. Mukhamedshina and A. A. Rizvanov, *Front. Neurosci.*, 2019, **13**, 163.
12 J. H. Heo, M. K. Kim, S. J. Lee and H. W. Kang, *Adv. Nanobiomed Res.*, 2025, **5**, 2500007.
13 O. G. De Jong, B. W. M. Van Balkom, R. M. Schiffelers, C. V. C. Bouten and M. C. Verhaar, *Front. Immunol.*, 2014, **5**, 608.
14 M. Garcia-Contreras, S. H. Shah, A. Tamayo, P. D. Robbins, R. B. Golberg, A. J. Mendez and C. Ricordi, *Sci. Rep.*, 2017, **7**, 1–10.
15 K. S. Leung, S. Shirazi, L. F. Cooper and S. Ravindran, *Cells*, 2022, **11**, 2851.
16 W. Li, Y. Liu, P. Zhang, Y. Tang, M. Zhou, W. Jiang, X. Zhang, G. Wu and Y. Zhou, *ACS Appl. Mater. Interfaces*, 2018, **10**, 5240–5254.
17 S. E. L. Andaloussi, S. Lakhal, I. Mäger and M. J. A. Wood, *Adv. Drug Delivery Rev.*, 2013, **65**, 391–397.
18 O. P. Wiklander, J. Z. Nordin, A. O'Loughlin, Y. Gustafsson, G. Corso, I. Mäger, P. Vader, Y. Lee, H. Sork, Y. Seow, N. Heldring, L. Alvarez-Erviti, C. I. Smith, K. Le Blanc, P. Macchiarini, P. Jungebluth, M. J. Wood and S. E. Andaloussi, *J. Extracell. Vesicles*, 2015, **4**, 26316.
19 L. Alvarez-Erviti, Y. Seow, H. Yin, C. Betts, S. Lakhal and M. J. A. Wood, *Nat. Biotechnol.*, 2011, **29**, 341–345.
20 S. A. A. Kooijmans, J. J. J. M. Gitz-Francois, R. M. Schiffelers and P. Vader, *Nanoscale*, 2018, **10**, 2413–2426.
21 J. Zou, M. Shi, X. Liu, C. Jin, X. Xing, L. Qiu and W. Tan, *Anal. Chem.*, 2019, **91**, 2425–2430.
22 S. S. Yerneni, S. Lathwal, P. Shrestha, H. Shirwan, K. Matyjaszewski, L. Weiss, E. S. Yolcu, P. G. Campbell and S. R. Das, *ACS Nano*, 2019, **13**, 10555–10565.
23 T. C. Pham, M. K. Jayasinghe, T. T. Pham, Y. Yang, L. Wei, W. M. Usman, H. Chen, M. Pirisinu, J. Gong and S. Kim, *J. Extracell. Vesicles*, 2021, **10**, e12057.
24 S. Mardpour, M. H. Ghanian, H. Sadeghi-Abandansari, S. Mardpour, A. Nazari, F. Shekari and H. Baharvand, *ACS Appl. Mater. Interfaces*, 2019, **11**, 37421–37433.
25 S. Lazar, S. Mor, J. Chen, D. Hao and A. Wang, *Extracell. Vesicles Circ. Nucleic Acids*, 2021, **2**, 175.
26 W.-Y. Quan, Z. Hu, H.-Z. Liu, Q.-Q. Ouyang, D.-Y. Zhang, S.-D. Li, P.-W. Li and Z.-M. Yang, *Molecules*, 2019, **24**, 2586.
27 Y. Liu, H. Meng, S. Konst, R. Sarmiento, R. Rajachar and B. P. Lee, *ACS Appl. Mater. Interfaces*, 2014, **6**, 16982–16992.
28 B. P. Lee, *Encyclopedia of Smart Materials*, 2022, vol. 1, pp. 66–73.
29 E. G. Tomarchio, R. Turnaturi, E. Saccullo, V. Patamia, G. Floresta, C. Zagni and A. Rescifina, *Bioorg. Chem.*, 2024, **150**, 107573.
30 S. H. Park, J. Y. Park, Y. B. Ji, H. J. Ju, B. H. Min and M. S. Kim, *Acta Biomater.*, 2020, **117**, 108–120.
31 D. G. Lim, R. E. Prim, E. Kang and S. H. Jeong, *Int. J. Pharm.*, 2018, **542**, 288–296.
32 S. H. Kim, J. H. Park, J. S. Kwon, J. G. Cho, K. G. Park, C. H. Park, J. J. Yoo, A. Atala, H. S. Choi, M. S. Kim and S. J. Lee, *Biomaterials*, 2020, **258**, 120267.
33 H. Lee, C. Kengla, H. S. Kim, I. Kim, J. G. Cho, E. Renteria, K. Shin, A. Atala, J. J. Yoo and S. J. Lee, *Adv. Healthc. Mater.*, 2024, **13**, e2302508.
34 S. X. Wang and J. H. Waite, *Nat. Rev. Chem.*, 2025, **9**, 159–172.
35 G. D. Prestwich, *J. Controlled Release*, 2011, **155**, 193–199.

